



Phytochrome B dynamics departs from photoequilibrium in the field

Romina Sellaro^{1†}  | Robert W. Smith^{2†} | Martina Legris³ | Christian Fleck^{2,4} | Jorge J. Casal^{1,3} 

¹Instituto de Investigaciones Fisiológicas y Ecológicas Vinculadas a la Agricultura (IFEVA), Facultad de Agronomía, Universidad de Buenos Aires and Consejo Nacional de Investigaciones Científicas y Técnicas (CONICET), Buenos Aires, Argentina

²Laboratory of Systems and Synthetic Biology, Wageningen UR, Wageningen, The Netherlands

³Fundación Instituto Leloir, Instituto de Investigaciones Bioquímicas de Buenos Aires, CONICET, Buenos Aires, Argentina

⁴Department of Biosystems Science and Engineering (D-BSSE), ETH-Zürich, Matthenstrasse 26, 4058 Basel, Switzerland

Correspondence

Jorge J. Casal, Instituto de Investigaciones Fisiológicas y Ecológicas Vinculadas a la Agricultura (IFEVA), Facultad de Agronomía, Universidad de Buenos Aires and Consejo Nacional de Investigaciones Científicas y Técnicas (CONICET), Buenos Aires C1417DSE, Argentina.
Email: casal@ifeva.edu.ar

Christian Fleck, Department of Biosystems Science and Engineering (D-BSSE), ETH-Zürich, Matthenstrasse 26, 4058 Basel, Switzerland.
Email: cfleck@ethz.ch

Present Address

Martina Legris, Center for Integrative Genomics, Faculty of Biology and Medicine, University of Lausanne, Lausanne CH-1015, Switzerland.

Funding information

FP7 Marie Curie Initial Training Network, Grant/Award Number: 316723 to R. W. S. 316723; Horizon 2020 Framework Programme, Grant/Award Number: 634942 to R. W. S.; Human Frontier Science Program, Grant/Award Number: RGP0025/2013 to C. F.; HFSP, Grant/Award Number: RGP0025/2013; Agencia Nacional de Promoción Científica y Tecnológica, Grant/Award Number: PICT-2015-1796; University of Buenos Aires, Grant/Award Number: 20020100100437

Abstract

Vegetation shade is characterized by marked decreases in the red/far-red ratio and photosynthetic irradiance. The activity of phytochrome in the field has typically been described by its photoequilibrium, defined by the photochemical properties of the pigment in combination with the spectral distribution of the light. This approach represents an oversimplification because phytochrome B (phyB) activity depends not only on its photochemical reactions but also on its rates of synthesis, degradation, translocation to the nucleus, and thermal reversion. To account for these complex cellular reactions, we used a model to simulate phyB activity under a range of field conditions. The model provided values of phyB activity that in turn predicted hypocotyl growth in the field with reasonable accuracy. On the basis of these observations, we define two scenarios, one is under shade, in cloudy weather, at the extremes of the photoperiod or in the presence of rapid fluctuations of the light environment caused by wind-induced movements of the foliage, where phyB activity departs from photoequilibrium and becomes affected by irradiance and temperature in addition to the spectral distribution. The other scenario is under full sunlight, where phyB activity responds mainly to the spectral distribution of the light.

KEYWORDS

light environment, phytochrome, shade avoidance, thermal reversion

† Sellaro, Romina and Smith, Robert should be considered joint first authors.

1 | INTRODUCTION

Plants sense features of the light environment to obtain information about the temporal and spatial conditions. Phytochrome B (phyB) is one of the most important photo-sensory receptors, able to sense light quantity (irradiance) and quality (spectral composition; Galvão & Fankhauser, 2015; Trupkin, Legris, Buchovsky, Rivero, & Casal, 2014). Phytochromes have two forms, P_r and P_{fr} . P_r is biologically inactive and has maximum absorbance at 660 nm (red light), whereas P_{fr} is biologically active and absorbs maximally at 730 nm (Burgie & Vierstra, 2014). Upon excitation, P_r transitions into the P_{fr} form (with rate k_1), and P_{fr} converts into the P_r form (with rate k_2 ; Mancinelli, 1994). This feature of phytochromes is central to the ability of phyB to perceive the threat imposed by nearby vegetation (Smith, 2000). Green leaves absorb strongly in red light but reflect and transmit most of the far-red light; therefore, the red/far-red ratio of the light decreases when the distance to the neighbours is reduced and the size of these neighbours is increased (Ballaré & Pierik, 2017; Casal, 2013; Franklin, 2008; Martínez-García et al., 2010). In turn, low-red/far-red ratios reduce the proportion of P_{fr} in the phytochrome molecule population. Therefore, the amount of P_{fr} depends on the characteristics of the surrounding vegetation canopy.

In the presence of neighbour signals, the reduced proportion of phyB P_{fr} triggers shade-avoidance and shade-acclimation responses. The shade avoidance syndrome includes increased stem and petiole growth, vertical (elevation) and horizontal displacement of the leaves, reduced branching, and early flowering, which are almost constitutive in *phyB* null mutants (Ballaré & Pierik, 2017; Casal, 2013; Franklin, 2008; Martínez-García et al., 2010). The ability of phytochrome to sense the red/far-red ratio to gather information about the canopy has been tested in the field. For instance, adding supplementary red light to the crown of grasses grown in a natural grassland to partially revert the naturally low-red/far-red ratios reaching the base of the plants enhances their tillering rate, which is a feature of plants grown in open places (Deregibus, Sanchez, Casal, & Trlica, 1985). Conversely, using neighbours or selective filters to reflect far-red light without shading the tagged plant initiates shade avoidance responses to the cues that the plant perceives as an early warning of neighbouring vegetation (Ballaré, Sánchez, Scopel, Casal, & Ghera, 1987). Actually, sensing the red/far-red ratio can help the plants accommodate the foliage in maize (Maddoni, Otegui, Andrieu, Chelle, & Casal, 2002) or sunflower crops (López, Sadras, Batista, Casal, & Hall, 2017), a response also observed among kin neighbours of *Arabidopsis* (Crepuy & Casal, 2015).

To regulate plant development, phyB molecules function as dimers. Systematic mathematical analysis of phyB dynamics and its physiological output has indicated that the active conformer of phyB is the P_{fr} - P_{fr} homodimer (D_2), whereas the P_{fr} - P_r heterodimer (D_1) and the P_r - P_r homodimer (D_0) are inactive (Klose et al., 2015). In addition to the photochemical reactions (k_1 and k_2), *Arabidopsis* phyB P_{fr} thermally reverts back to P_r in a light-independent reaction that occurs at a slower rate between P_{fr} - P_{fr} and P_{fr} - P_r (k_{r2}) compared with the faster rate of reversion between P_{fr} - P_r and P_r - P_r (k_{r1}). Within a cell, phyB activity correlates with the levels of D_2 in the nucleus. A mathematical model describing the behaviour of D_2 incorporates the

transition rates k_1 , k_2 , k_{r1} , and k_{r2} as well as subcellular events such as the rate of phyB synthesis, degradation, and translocation from the cytosol to the nucleus. We shall refer to this as the “cellular model” of phyB (Klose et al., 2015). This larger system can be simplified into the so-called “three-state model” that describes solely the conformational changes between D_0 , D_1 , and D_2 by ignoring cellular compartments, phyB synthesis, and degradation. By simplifying the model, it is possible to analytically approximate the relationship between changing environments with levels of D_2 and phyB activity (Legris et al., 2016).

Recent observations have indicated that phyB can act as a temperature sensor (Jung et al., 2016; Legris et al., 2016). Whereas k_1 and k_2 depend on the light input, k_{r1} and k_{r2} depend on temperature. Therefore, the level of D_2 increases with the red/far-red ratio, as a result of changes to the ratio between k_1 and k_2 , and decreases with temperature in the physiological range because warm temperatures increase k_{r1} and k_{r2} . Cellular features correlated with phyB activity such as the pattern of phyB nuclear bodies (Legris et al., 2016) and the amount of phyB associated to DNA (Jung et al., 2016) respond to temperature. The physiological output mediated by phyB is better accounted for by growth models that incorporate the impact of temperature on D_2 calculations (Legris et al., 2016).

Although it is clear that phyB is important to perceive neighbouring vegetation in the field, our knowledge of the phyB dynamics under field conditions is scant. Before the presence of different phytochrome genes had been documented, phyA was used to measure spectroscopically the impact of either canopy shade (Holmes & Smith, 1977) or neighbour plants reflecting far-red light on the proportion of P_{fr} in cuvettes containing etiolated tissues (Smith, Casal, & Jackson, 1990). The effects of the light environment on phytochrome status were typically summarized in the photoequilibrium or $P_{fr}/(P_{fr} + P_r)$ ratio, which is either estimated by a calibration curve of photoequilibrium against red/far-red ratio or calculated as $k_1/(k_1 + k_2)$ (Holmes & Smith, 1977; Mancinelli, 1988, 1994). This is a simplification that ignores other cellular processes that can affect phyB status.

The aim of this paper is to use the available mathematical tools to describe the dynamics of phyB activity under field conditions. Current questions include the extent of quantitative dependence of phyB activity on the level of irradiance and temperature under field conditions. At high irradiance, k_1 and k_2 are predicted to become dominant over k_{r1} and k_{r2} , and therefore, temperature-dependence of phyB would be minimized. At low irradiance, phyB activity would become irradiance and temperature-dependent due to the increased importance of thermal reversion (mainly k_{r1}) relative to light-dependent reactions. However, the range of irradiances where phyB is dominated by one scenario or the other is not clear at present.

2 | MATERIALS AND METHODS

2.1 | Light measurements

The light environment was scanned at 1-nm resolution between 400 and 800 nm with a spectroradiometer (FieldSpec Pro FR; Analytical

Spectral Devices [ASD]). The remote probe of the spectroradiometer was placed at the indicated time of the day and position within or outside the canopy. All the field scans are presented in Table S1. Light conditions for laboratory experiments were as described (Legris et al., 2016).

2.2 | Basic simulations of the cellular D_2 model

To simulate the dynamics of nuclear D_2 , we used the published model of phyB dynamics in etiolated seedlings (Klose et al., 2015). The parameters for the model are given in Table S2, and the system is initially set such that all phyB is in the P_r - P_r (D_0) form in the cytoplasm.

Light conditions enter the model via the reaction rates of P_r to P_{fr} (k_1) and P_{fr} to P_r (k_2) conversion. To do this, we took the measured spectral photon distribution (I_λ in $\mu\text{mol m}^{-2} \text{s}^{-1}$) from the different canopy conditions and multiplied these values by the photoconversion spectra of phyB (σ_λ^r for the P_r to P_{fr} reaction and σ_λ^{fr} for the P_{fr} to P_r reaction in $\text{m}^2 \text{mol}^{-1}$; Mancinelli, 1994). Because the model was simulated over diurnal cycles of varying light intensity (see below) the k_1 and k_2 values become time-dependent:

$$k_1(t) = 60 \frac{\text{s}}{\text{min}} \times 10^{-6} \frac{\text{mol}}{\mu\text{mol}} \times \sum_{i=\lambda_{\min}}^{\lambda_{\max}} (I_i(t) \times \sigma_i^r), \quad (1)$$

$$k_2(t) = 60 \frac{\text{s}}{\text{min}} \times 10^{-6} \frac{\text{mol}}{\mu\text{mol}} \times \sum_{i=\lambda_{\min}}^{\lambda_{\max}} (I_i(t) \times \sigma_i^{fr}), \quad (2)$$

where λ_{\max} and λ_{\min} are the longest (800 nm) and shortest (400 nm) wavelength of the measured spectral photon distribution. The measured spectral photon distributions were interpolated such that the system could be simulated every minute. After the last measured time point, we assume that the plants are under darkness and thus $k_1 = k_2 = 0$.

2.3 | Simulating D_2 under fluctuating environments

In the case of recording D_2 under diurnal field conditions, the simulated levels of D_2 were obtained by simulating the cellular model (Klose et al., 2015) for three 10-h $50\text{-}\mu\text{mol m}^{-2} \text{s}^{-1}$ light to 14-h dark diurnal cycles ($k_1 = 5.15 \text{ min}^{-1}$, $k_2 = 1.79 \text{ min}^{-1}$) followed by 1 day of varying light intensity using the time-dependent functions of k_1 and k_2 described above. The time-dependent changes in light intensity were interpolated to vary each minute rather than on the measured hour timescale.

To obtain simulated levels of D_2 under rapidly fluctuating environments, the same procedure was performed without interpolation of measured light distributions as measurements of varying light intensity were recorded each second.

2.4 | Relating irradiance to D_2 levels

The simulated levels of D_2 were obtained by simulating the cellular model (Klose et al., 2015) for three 10-h $50\text{-}\mu\text{mol m}^{-2} \text{s}^{-1}$ light to 14-h dark diurnal cycles ($k_1 = 5.15 \text{ min}^{-1}$, $k_2 = 1.79 \text{ min}^{-1}$) followed by 6 h under the different experimental light conditions. The recorded level of D_2 is the average level from this 6-h period.

2.5 | Sensitivity analysis of the cellular D_2 model

Sensitivity analysis of the phyB model was conducted by fixing 11 of the 12 model parameters to their optimal value (Table S2) and varying the one "open" parameter between 10^{-1} and 10 times its optimal value. The model was simulated for 3 days under laboratory conditions before a single diurnal cycle using time-dependent measured spectral photon irradiances of the light at the top and bottom of the canopy. The total amount of nuclear D_2 produced was then recorded relative to simulations performed with the optimal parameter set.

2.6 | Calculation of D_2 with the three-state model

According to the three-state model, which only incorporates the photochemical reactions and thermal reversion, the proportion of phyB as D_2 can be calculated:

$$D_2 = \frac{2k_1^2}{2k_1^2 + 2k_1(2k_2 + 2k_{r2}) + (k_2 + k_{r1})(2k_2 + 2k_{r2})}. \quad (3)$$

The proportion of D_2 at photoequilibrium was calculated by using Equation (3) without thermal reversion ($k_{r1} = k_{r2} = 0$). To calculate k_1 and k_2 , we used photoconversion cross-section data from Mancinelli (1994) as in the case of the cellular model, except for Figure 9 where we used cross-section data from Kelly and Lagarias (1985) because the latter data set had been used to calculate k_{r1} and k_{r2} under different temperatures (Jung et al., 2016; Legris et al., 2016).

2.7 | Hypocotyl growth measurements

For hypocotyl growth, we used seedlings of the wild-type (WT) Landsberg *erecta*, of the *phyB-5* null mutant (formerly *hy3-8-36*, Koornneef, Rolf, & Spruit, 1980). Seeds were sown on clear plastic boxes containing 0.8% agar water and incubated 3–5 days at 4 °C in darkness. Stratified seeds were transferred to white light, $50 \mu\text{mol m}^{-2} \text{s}^{-1}$ provided by fluorescent tubes, photoperiod 10 hr, and 20 °C for 3 days. For the measurements of hypocotyl growth rate under natural radiation, at the beginning of the fourth day, light-grown seedlings were transferred either to unfiltered sunlight or to the different canopy shade conditions. We photographed the seedlings with a digital camera at the beginning of the fourth day and 8 h later. We measured hypocotyl length using image-processing software, and the length increment was divided by 8 h to obtain hourly rates. Growth measurements under laboratory conditions correspond to the previously published database (Legris et al., 2016), where the seedlings were treated in a similar way as described for the experiments under natural radiation with the exception that they were transferred to the different irradiances and photographed 1 h after the beginning of the photoperiod of the fourth day and photographed again 9 h later. The hourly rates were calculated by dividing the length increments by 9 hr.

2.8 | Predicting growth rates

To predict hypocotyl growth rates, we used the function proposed by Legris et al. (2016), where growth depends on the activity of phyB, the activity of other photoreceptors, and the temperature of the environment. We assume, as in Klose et al. (2015), that D_2 in the nucleus

(nucleoplasm and nuclear bodies) are the active components of the phyB model that regulate growth.

To estimate the D_2 values incorporated into the growth model, the dynamics of nuclear D_2 were simulated for three 10-h 50- $\mu\text{mol m}^{-2} \text{s}^{-1}$ light to 14-h dark diurnal cycles ($k_1 = 5.15 \text{ min}^{-1}$, $k_2 = 1.79 \text{ min}^{-1}$) followed by the treatment condition the subsequent day. In laboratory experiments, during the fourth day the system was simulated for 1 h under 50 $\mu\text{mol m}^{-2} \text{s}^{-1}$ before 9 h of the experimental condition (either 10 $\mu\text{mol m}^{-2} \text{s}^{-1}$ or maintained in 50 $\mu\text{mol m}^{-2} \text{s}^{-1}$). In experiments under natural radiation, during the fourth day, the system was simulated for the 8 h under the experimental condition (sunlight or various shade conditions). Growth was then predicted using the mean amount of nuclear D_2 during the 9 or 8 h of experimental conditions. To simulate growth of *phyB* null plants, the growth function was calculated without any nuclear D_2 present. To simulate growth of the *phyB*^{R582A} mutant, the dark reversion rate of phyB was set to 10% of its WT value. This difference of dark reversion rate between *phyB*^{WT} and *phyB*^{R582A} was predicted by fitting exponential decay functions ($P_{fr}(t) = \alpha e^{-\beta t}$) to the dark reversion data presented in Figure 2b of Zhang, Stankey, and Vierstra (2013) and comparing the rate β , that is, $\beta^{\text{WT}} = 10\beta^{\text{R582A}}$.

2.9 | Analysis of phyB nuclear bodies

For confocal microscopy, we used transgenic lines expressing *phyB*-YFP (Burgie & Vierstra, 2014; Zhang et al., 2013). These lines express the WT *PHYB* cDNA with the cDNA encoding YFP fused to the 3' end, under the control of the *UBQ10* promoter in the *phyB*-9 background. Confocal images were taken with an LSM5 Pascal microscope (Zeiss), equipped with a 40 \times water immersion objective (C-Apochromat 40 \times /1.2; Zeiss). For GFP, visualization probes were excited with an argon laser (488 nm), and fluorescence was detected with a BP 505–530 filter. Pictures of individual nuclei were taken from the epidermis and first subepidermal layers of the hypocotyl.

Image analysis was performed in batch with an image segmentation program developed in Icy (<http://icy.bioimageanalysis.org/>). Nuclei limits were identified using the HK means segmentation method, a region of interest (ROI) was created, and size and mean grey value were measured inside it. Afterwards, into each nucleus, NBs were detected using the wavelet spot detector, one ROI per granule was generated, and size and mean grey value of each granule were recorded. Nucleoplasm was defined as an ROI resulting from the subtraction of the nuclear ROI minus all the NB ROIs, and area and mean grey value were measured inside this nucleoplasm ROI.

2.10 | Predicting the proportion of phyB in nuclear bodies

The simulated amount of phyB within nuclear bodies was recorded using the cellular model (Klose et al., 2015) after 4 h of the experimental light conditions (varying red/far-red ratios or irradiances).

2.11 | Calculating PAR required for obtaining maximum D_2 values

To calculate the instantaneous photosynthetically active radiation (PAR, 400–700 nm, $\mu\text{mol m}^{-2} \text{s}^{-1}$) required to establish nuclear D_2 levels close to photoequilibrium, the cellular model was simulated for 2 days under constant light conditions corresponding to the measured spectral photon distribution at different heights of the wheat canopy at midday. Each spectral photon distribution was used at a wide range of irradiances (by multiplying each one of the wavelengths by the same factor) to generate a curve of response of D_2 to irradiance. The PAR value under each simulated condition that corresponded to the nucleus containing 99% of the nuclear D_2 at photoequilibrium was then recorded.

3 | RESULTS

3.1 | Sensitivity of the model parameters in the estimation of D_2

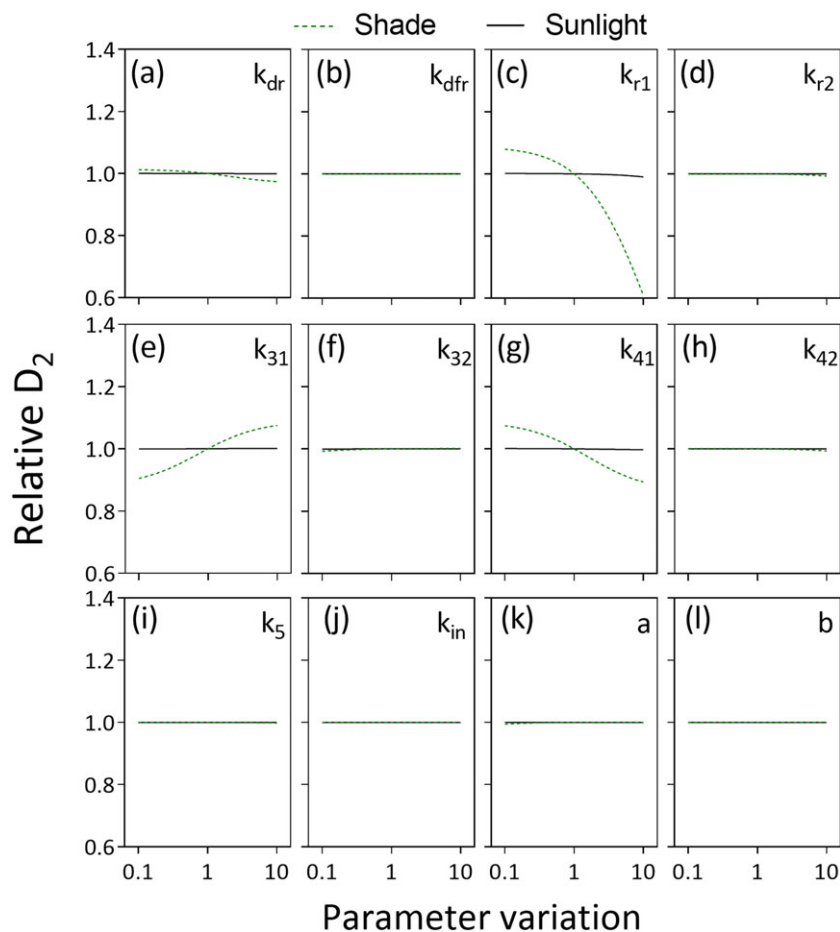
The *phyB* cell model has been developed for etiolated seedlings exposed to different wavelengths of continuous light within the red and far-red range (Klose et al., 2015). However, our aim is to predict the dynamics of *phyB* in light-grown plants exposed to white light/night cycles, because these are the plants that elicit shade-avoidance responses. The developmental context could affect processes that control the D_2 levels and to focus the analysis on the most influential parameters we investigated their impact on D_2 . For this purpose, we used the model to calculate nuclear D_2 varying one parameter at the time within a wide range (10⁻¹ to 10 fold the original rate) in combination with light spectra corresponding to sunlight or to canopy shade. Under shade, the most influential parameters were the rate of D_1 to D_0 dark reversion (k_{r1}), the rate of D_1 nuclear body (NB) association (k_{31}), and the rate of D_1 NB dissociation (k_{41} ; Figure 1). However, under sunlight, no parameter perturbation had a significant influence on simulated D_2 .

3.2 | Analysis of hypocotyl growth to test the parameters that estimate D_2

The rate of dark reversion (Enderle et al., 2017; Kim et al., 2004; Smith et al., 2017) and the formation of *phyB* NBs (Bauer et al., 2004) are two features of the *phyB* system that can be affected by biochemical interactions and developmental context. Because the parameters that are most influential for D_2 estimation (k_{r1} , k_{31} , and k_{41}) are actually associated to dark reversion and *phyB* NB dynamics, we investigated the impacts of k_{r1} , k_{31} , and k_{41} on the estimation of biological outputs under the shade-avoidance conditions (i.e., in light-grown seedlings).

For this purpose, we used the nuclear D_2 values estimated by the *phyB* cellular model in combination with a hypocotyl growth model (which uses D_2 as input) to predict hypocotyl growth rates. De-etiolated *Arabidopsis thaliana* seedlings of the WT and of the *phyB* null mutant were grown in the glasshouse, under different conditions of natural shade. We also used data corresponding to seedlings of the WT and of the *phyB* mutant complemented with a mutated *phyB* that

FIGURE 1 Sensitivity analysis of nuclear D_2 cellular model parameters when simulated under sunlight or canopy shade conditions (Table S1, sunlight and wheat 0 cm at 13:00). In each simulation, 11 of 12 model parameters were fixed to their original value, whilst one was changed to between 10^{-1} and 10 times its original value. After each simulation, the total amount of D_2 in the nucleus was recorded. (a) k_{dr} = phyB degradation; (b) k_{dfr} = P_{fr} -enhanced degradation; (c) k_{r1} = D_1 dark reversion; (d) k_{r2} = D_2 dark reversion; (e) k_{31} = D_1 NB association; (f) k_{32} = D_2 NB association; (g) k_{41} = D_1 NB dissociation; (h) k_{42} = D_2 NB dissociation; (i) k_5 = D_0 NB dissociation; (j) k_{in} = P_{fr} nuclear import; (k) a = ratio of phyB and interaction partner synthesis rates; (l) b = ratio of nuclear import and degradation rate of interaction partner. Both parameters “ a ” and “ b ” are related to phyB P_{fr} -enhanced degradation (see Table S2) [Colour figure can be viewed at wileyonlinelibrary.com]



shows reduced dark reversion (phyB^{R582A}; Zhang et al., 2013) grown under different irradiances of white light under controlled conditions to include genetically modified phyB activity in the test (from the database published by Legris et al., 2016). We analysed the goodness of fit of the model (denoted by chi-square values) as affected by the modification of k_{r1} , k_{31} , and k_{41} . The lowest chi-square values were observed when previously optimized values of k_{r1} were multiplied by 9.77 (Figure 2a). This indicates that D_1 dark reversion to D_0 would be faster in de-etiolated compared with etiolated seedlings.

For k_{31} and k_{41} , the same minimal chi-square value was not attained within the range of analysis (10^{-1} to 10 fold the previously optimized rate). However, chi-square values were reduced either by lowering the rate of NB association (k_{31}) or by increasing the rate of NB dissociation (k_{41} ; Figure 2a). Because phyB within NBs is considered to be protected from dark reversion (Klose et al., 2015; Rausenberger et al., 2010; Van Buskirk, Reddy, Nagatani, & Chen, 2014) and lower k_{31} or higher k_{41} imply a reduction of phyB within NBs, the changes in k_{31} and k_{41} that increase goodness of fit also increase the rates of apparent dark reversion in de-etiolated compared with etiolated seedlings. Because fitting to growth data is improved by moving k_{r1} , k_{31} , and k_{41} towards a direction that implies a faster thermal reversion of D_1 , we used the cell model to estimate D_2 based on k_{r1} multiplied by 9.77. We do not claim that the real k_{r1} is 9.77-fold higher but simply that this change summarizes diverse features of the model that would result in a less stable D_1 (see Section 4). Therefore, we will call D_2' the estimates produced by the perturbed model and D_2° those generated by the unperturbed model. The relationship

between observed and predicted growth values using D_2' is presented (Figure 2b).

3.3 | Analysis of phyB subnuclear distribution to test the parameters that estimate D_2

Following the analysis of the impacts of k_{r1} , k_{31} , and k_{41} on the estimation of biological outputs under the shade-avoidance conditions, we used the cell model to estimate the proportion of phyB in NBs. As expected, increasing either the red/far-red ratio or the irradiance of white light increased the proportion of phyB in NBs in light-grown seedlings of *A. thaliana* expressing phyB fused to GFP (Figure 3a,b). There is substantially less phyB in NBs of light-grown seedlings than predicted by the cellular model developed for etiolated seedlings (Figure S1) and the average ratio between observed and predicted proportion of phyB in NBs is 0.22 ± 0.02 (mean \pm SE). We analysed the goodness of fit of the cellular model to predict the proportion of phyB in NBs (denoted by chi-square values) as affected by the modification of k_{r1} , k_{31} , or k_{41} . The performance of the model was improved by increasing k_{r1} or k_{41} or by decreasing k_{31} (Figure 3c). Therefore, contrasting model predictions and observations of either growth or phyB NB dynamics yields consistent results.

3.4 | Simulated D_2 under different canopy conditions

To describe the impact of light conditions in the field on the level of active phyB, we present three values: D_2° (estimated by the cellular

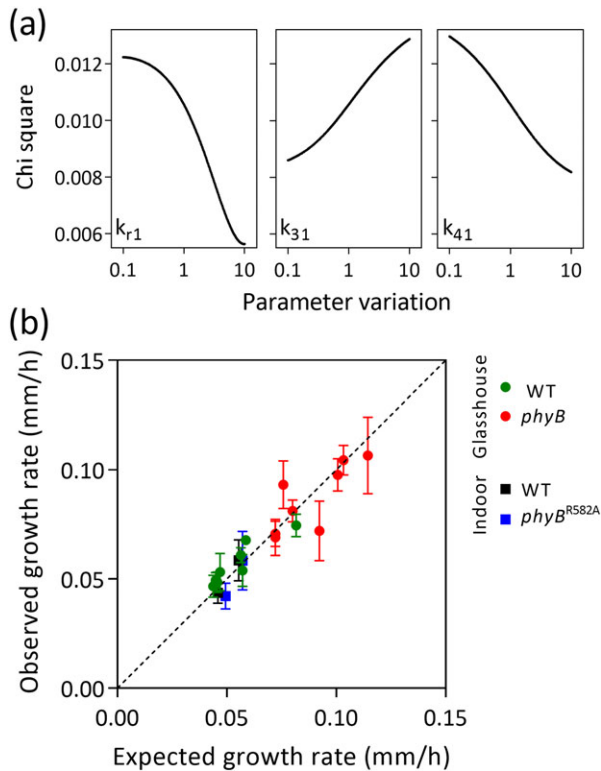


FIGURE 2 Goodness of fit of hypocotyl extension growth predictions as affected by variations in parameters of the D_2 cellular model. (a) Chi-square values when k_{r1} , k_{31} , or k_{41} were changed to between 10^{-1} and 10 times their original values. (b) Observed growth rates plotted against the calculated values using the optimum value of k_{r1} from (a). De-etiolated seedlings of *Arabidopsis thaliana* were grown for one photoperiod (10 hr) either in a glasshouse, under sunlight, and different canopy shade conditions, or in the laboratory, under different irradiances of white light. Glasshouse experiments include the WT and $phyB$ null mutant (means and SE of eight seedlings under each condition). Laboratory experiments include the WT and the $phyB$ mutant complemented with $phyB^{R582A}$ whose dark reversion rate is 10% that of WT $phyB$ (data from Legris et al., 2016) [Colour figure can be viewed at wileyonlinelibrary.com]

model), D_2' (estimated by the cellular model with k_{r1} multiplied by 9.77), and D_2 at photoequilibrium (D_2^P , estimated by the three-state model, Equation (3), excluding dark reversion, i.e., $k_{r1} = k_{r2} = 0$). D_2' is provided because it improves the prediction of hypocotyl growth in de-etiolated seedlings, and D_2^P because P_{fr} levels at photoequilibrium have traditionally been used to describe phytochrome status (Mancinelli, 1988, 1994; Smith & Holmes, 1977). At photoequilibrium, the status of phytochrome is determined solely by the photochemical reactions and depends exclusively on the spectral photon distribution of the light, but due to the other reactions incorporated in the cellular model, the steady-state level of D_2 may depart from photoequilibrium. To investigate the light conditions that enhance this divergence, we scanned the light reaching the bottom of a series of canopies with different floristic composition at midday. We ordered the stations by increasing values of the integral of irradiance in the red plus far-red wavebands (600–800 nm, although D_2 calculations are based on 400- to 800-nm data, we selected the most influential wavebands for the x-axis; Figure 4a). Despite fluctuations in the D_2^P due to the differences in spectral photon distribution, the difference between

D_2^P and steady-state D_2' values decreased steadily with irradiance (Figure 4b). As expected, D_2° showed intermediate values.

3.5 | Diurnal dynamics of D_2 under field conditions

To describe the dynamics of active $phyB$ in the field, we produced scans of the light reaching different positions above or beneath either sorghum or wheat canopies at different times of the day. We summarized the light information in terms of PAR (Figure 5a) and red/far-red ratio (Figure 5b). Above the canopy (unfiltered sunlight), both D_2° and D_2' were very close to D_2^P throughout the whole photoperiod, with minor deviations at the extremes of the day (Figure 5c). However, under the shade of any of the two canopies, D_2' was significantly lower than D_2^P at any time of the day, but more intensively at the extremes of the photoperiod, when light levels are reduced (Figure 5c).

3.6 | Dynamics of D_2 under fluctuating light conditions

Light can penetrate through gaps within the canopy and due to the movement of the foliage induced by the wind, whereas the position of these gaps is not static. Therefore, in the understory of the canopy, plants can be exposed to sunflecks, which persist for seconds. Instead of averaging several scans within a given area, a procedure that tends to eliminate this source of variability, we continually recorded scans of the light environment for 10 min at a single position within the canopy. Figure 6a,b describes the rapid fluctuations in PAR and red/far-red ratio. We continuously simulated D_2° and D_2' and calculated D_2^P under these conditions. As expected, D_2^P faithfully followed the fluctuations in red/far-red ratio. At the maximum peaks, D_2' was lower than D_2^P (with D_2° assuming intermediate values) as observed for static measurements (Figures 4 and 5). Conversely, at the lowest red/far-red ratios, D_2^P was lower than D_2' or D_2° . This is likely to reflect the inertia generated by the reactions involved in the cell model. Therefore, although $phyB$ activity will be affected by rapid light fluctuations within the canopy, the rate of the reactions attenuates the impact of these fluctuations on the $phyB$ steady state.

3.7 | Simulated D_2 under cloudy skies

To investigate the impact of cloudiness on $phyB$ activity, we recorded scans of the light out of the canopy and under shade, both at midday (Figure 7a). The measurements of sunlight out of leaf shade come from different winter days, and some changes in spectral distribution generated minor fluctuations in D_2^P . More importantly, the reduced irradiance (PAR) caused by denser nubosity significantly lowered D_2° and D_2' compared with D_2^P (Figure 7b). This indicates that clouds can affect the status of $phyB$ out of the canopy even at midday. D_2^P increased within the canopy with increasing cloudiness. This is caused by the reduced proportion of direct compared with diffuse sunlight when clouds cover the solar disk. Diffuse light can penetrate the canopy through gaps and reach lower strata of the canopy with a higher red/far-red ratio, except under sunflecks, where direct light penetrates through the gaps.

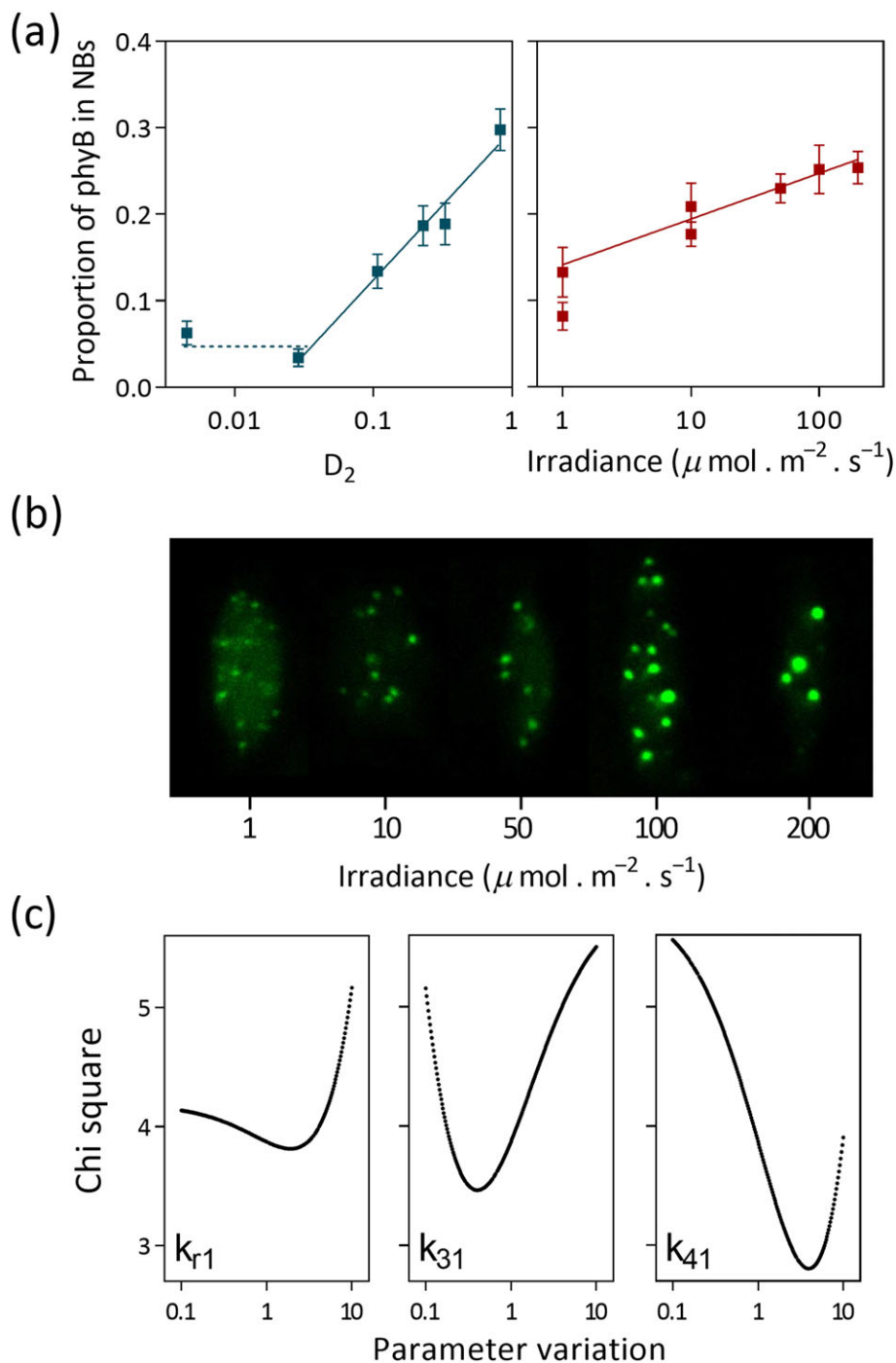


FIGURE 3 Goodness of fit of the predictions of the proportion of phyB in NBs as affected by variations in parameters of the D_2 cellular model. (a) Higher red/far-red ratios or irradiances of white light increase the proportion of phyB in NBs. (b) Representative images of the responses to irradiance. (c) Chi-square values when k_{r1} , k_{31} , or k_{41} were changed to between 10^{-1} and 10 times their original values. De-etiolated seedlings of *Arabidopsis thaliana* were exposed either to different red/far-red ratios or different irradiances of white light for 4 h before analysis by confocal microscopy (means and SE of 13 seedlings under each condition) [Colour figure can be viewed at wileyonlinelibrary.com]

3.8 | Irradiance required to achieve maximum D_2 steady-state levels

We investigated the irradiance required to achieve values of nuclear D_2 close to D_2^P for given a spectral composition. For this purpose, we used the scans obtained at different heights of a wheat canopy, in combination with the cellular model to estimate D_2' and D_2° . All the wavelengths of a given scan were multiplied by a factor to either

increase or decrease the irradiance integral and build up D_2' and D_2° response curves to irradiance for each spectral distribution. In Figure 8, we plot the irradiance at which D_2' or D_2° equals $0.99 D_2^P$. This irradiance is expressed in terms of PAR (400–700 nm) because this is a common determination in plant canopies and is plotted against D_2^P for a given spectral distribution. The irradiance to reach maximum $0.99 D_2^P$ was in the range of 200–300 $\mu\text{ mol} \cdot \text{ m}^{-2} \cdot \text{ s}^{-1}$ when the calculations are based on D_2' .

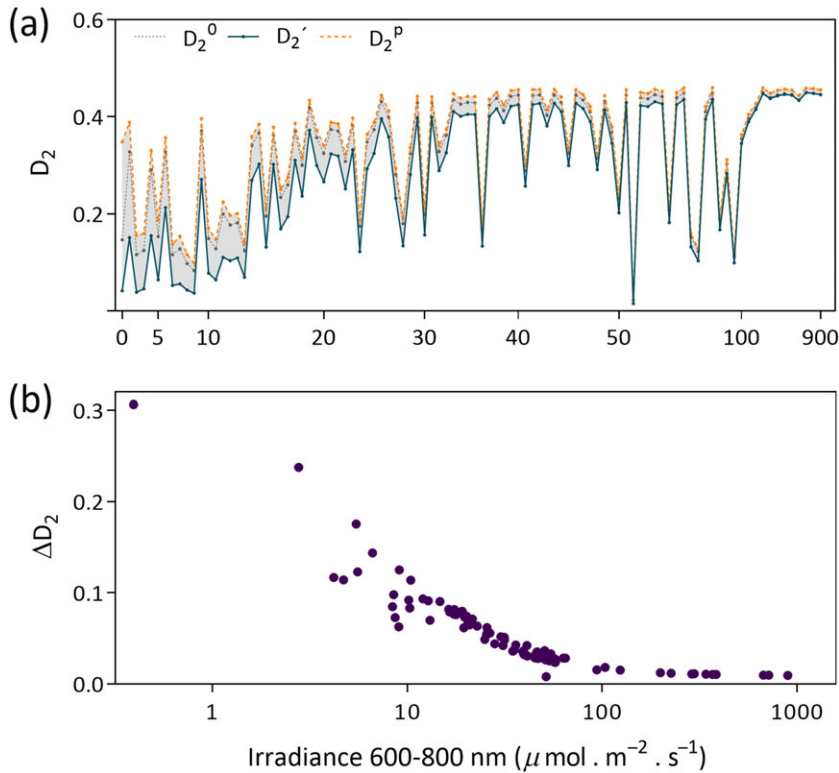


FIGURE 4 Nuclear D_2 departs from photoequilibrium under low irradiances. (a) Nuclear D_2 estimated by the original (D_2^0) or the perturbed model (D_2') compared with D_2 at photoequilibrium (D_2^P) for different canopy conditions. Each point represents a different canopy condition ordered according to the red plus far-red light (600–800 nm) irradiance (increasing towards the right). (b) Difference between D_2^P and D_2' plotted against the red plus far-red irradiance (calculated from data in a) [Colour figure can be viewed at wileyonlinelibrary.com]

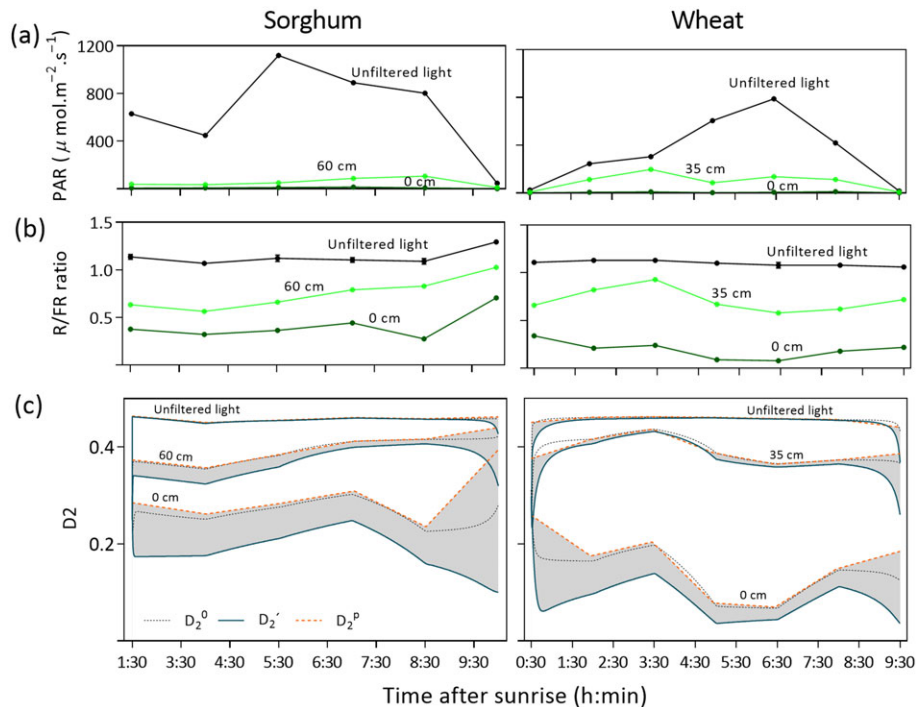


FIGURE 5 Time course of nuclear D_2 under sunlight and different heights within vegetation canopies during the photoperiod. (a,b) PAR (a, irradiance between 400 and 700 nm) and red (R, between 650 and 670 nm)/far-red (FR, between 720 and 740 nm) ratio (b) above or beneath sorghum and wheat canopies (the heights within the canopies are indicated). Data are means of three replicates \pm SE (often smaller than the symbols) (c) nuclear D_2 estimated by the original (D_2^0) or the perturbed model (D_2') compared with D_2 at photoequilibrium (D_2^P) for the conditions described in (a,b). The grey area shows the difference between D_2^P and D_2' [Colour figure can be viewed at wileyonlinelibrary.com]

3.9 | Impact of temperature on active phyB in the field

Currently, there is no information available to describe the response of all the parameters of the cellular model to temperature because

this model was constructed using data measured at room temperature (22 °C). Therefore, we used the three-state model of phyB to describe the short-term impact of temperature, that is, within a time frame where phyB synthesis, degradation, and nuclear accumulation would not be significantly affected by temperature. As expected, due

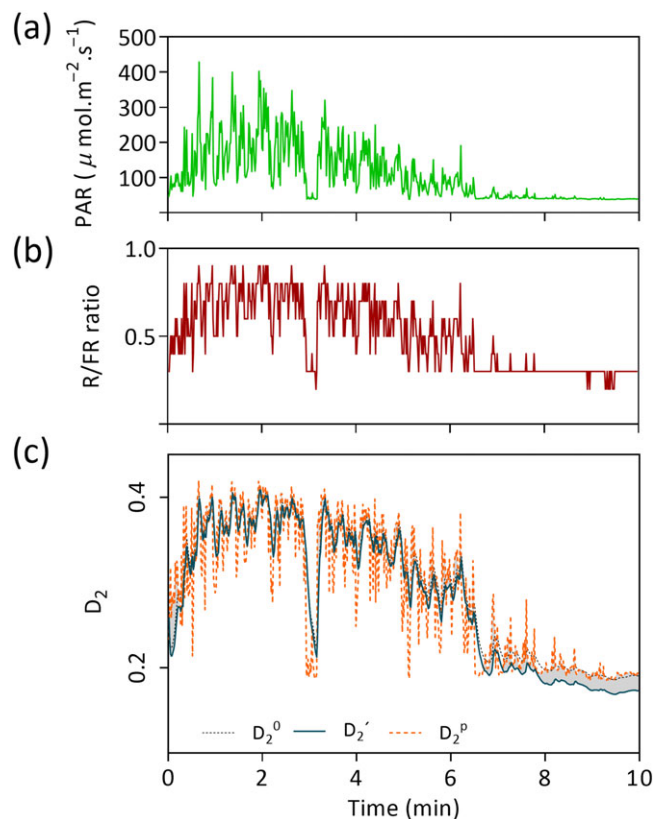


FIGURE 6 Kinetics of nuclear D_2 under rapid fluctuations of light conditions under a grass canopy. (a,b) Time course of the PAR (a, irradiance between 400 and 700 nm) and red (R, between 650 and 670 nm)/far-red (FR, between 720 and 740 nm) ratio (b). (c) Nuclear D_2 estimated by the original (D_2^0) or the perturbed model (D_2') compared with D_2 at photoequilibrium (D_2^p) for the conditions described in (a,b). The grey area shows the difference between D_2^p and D_2' (positive values). Time = 0 indicates the beginning of the measurements; the experiment was conducted at midday [Colour figure can be viewed at wileyonlinelibrary.com]

to the increased rates of thermal reversion under warmer temperatures (Jung et al., 2016; Legris et al., 2016), the PAR required to reach the maximum D_2 values established by a given spectral composition increased with temperature, from approximately $100 \mu\text{mol m}^{-2} \text{s}^{-1}$ at 10°C to approximately $600 \mu\text{mol m}^{-2} \text{s}^{-1}$ at 30°C (Figure 9).

4 | DISCUSSION

Phytochrome can sense subtle changes in light conditions such as the reflection of far-red light by nearby vegetation, which slightly reduces the red/far-red ratio before there is actual shading among neighbours (Ballaré et al., 1987; Ballaré, Scopel, & Sánchez, 1990; Casal, Sanchez, & Deregibus, 1986). This function is mediated predominantly by phyB (Smith & Whitelam, 1990; Yanovsky, Casal, & Whitelam, 1995). The perception of the light cues of neighbouring vegetation plays a fundamental role in the adjustment of plant plastic growth and development to the prevailing conditions both in natural canopies and in crops. The system has achieved such degree of sophistication that even exposure of the tip of a rosette leaf is enough to induce its vertical repositioning

away from the soil, where it would be more likely to become shaded (Michaud, Fiorucci, Xenarios, & Fankhauser, 2017; Pantazopoulou et al., 2017). The precision of the system is illustrated by the observation that minor differences in the vertical light profile generated by a neighbour cause the horizontal reorientation of leaves to minimize mutual shading among kin neighbours, a response that is not initiated with nonkin (Crepny & Casal, 2015). Given this scenario, it is important to understand the dynamics of phyB under natural radiation. To address this issue, we have used a cellular model of phyB that incorporates the rates of photochemical reactions between P_r and P_{fr} and vice versa, the rates of P_{fr} to P_r thermal reversion, and the rates of synthesis, degradation, translocation to the nucleus, and assembly/disassembly from NBs (Klose et al., 2015). We were able to define two different scenarios under natural radiation conditions: One where the proportion of phyB in its active conformer, nuclear D_2 , depends almost exclusively on the red/far-red ratio; the other where nuclear D_2 depends not only on the red/far-red ratio but also on irradiance. The upper limit of the second scenario is set by the conditions where the irradiance measured as a red plus far-red integral (600–800 nm) is at approximately $200 \mu\text{mol m}^{-2} \text{s}^{-1}$ at 20°C (Figure 4). Expressed in terms of PAR (400–700 nm), which does not fully overlap the spectral region of maximum phyB absorbance but is a frequently used measurement of irradiance in plant canopies, this upper limit would be at approximately $200\text{--}300 \mu\text{mol m}^{-2} \text{s}^{-1}$ at 20°C (Figure 8). By using the three-state model of phyB, based only on photochemical reactions and thermal reversion (the rest of the parameters of the cellular model are only available for 20°C), the upper limit can be extended up to a PAR of $600 \mu\text{mol m}^{-2} \text{s}^{-1}$ at 30°C (Figure 9). In other words, this indicates that low irradiances would reduce the proportion of D_2 in the nucleus under canopy shade throughout the photoperiod and out of the canopy under cloudy skies and at the extremes of the photoperiod (Figures 5 and 7). The phyB-mediated responses to irradiance and to ambient temperature are two faces of the same coin because both depend on P_{fr} to P_r reversion (Legris, Nieto, Sellaro, Prat, & Casal, 2017). The impact of P_{fr} to P_r thermal reversion becomes diluted with increasing rates of photochemical reactions, and therefore, phyB would not be a major temperature sensor above the aforementioned irradiance levels.

Natural canopies are dynamic at different timescales ranging from weeks as a result of the growth of different plants that compose the stand, to seconds, as wind causes the movement of leaves and the transient penetration of sunflecks (Kaiser, Morales, & Harbinson, 2017). We have analysed how photo-sensory receptors respond to relatively extended interruptions of shade (Moriconi et al., 2018; Sellaro, Yanovsky, & Casal, 2011), but we still do not know how they integrate rapid shade/sunfleck/shade transitions. By using the model, we can predict that cellular reactions impose a certain delay and attenuation of the fluctuations of D_2 in response to these transients (Figure 6). These observations are consistent with previous reports based on spectrophotometric measurements of phytochrome in etiolated seedlings, which show that photoequilibrium is achieved within 5 s under full sunlight and only after approximately 30 s under deep canopy shade (Holmes & Smith, 1977).

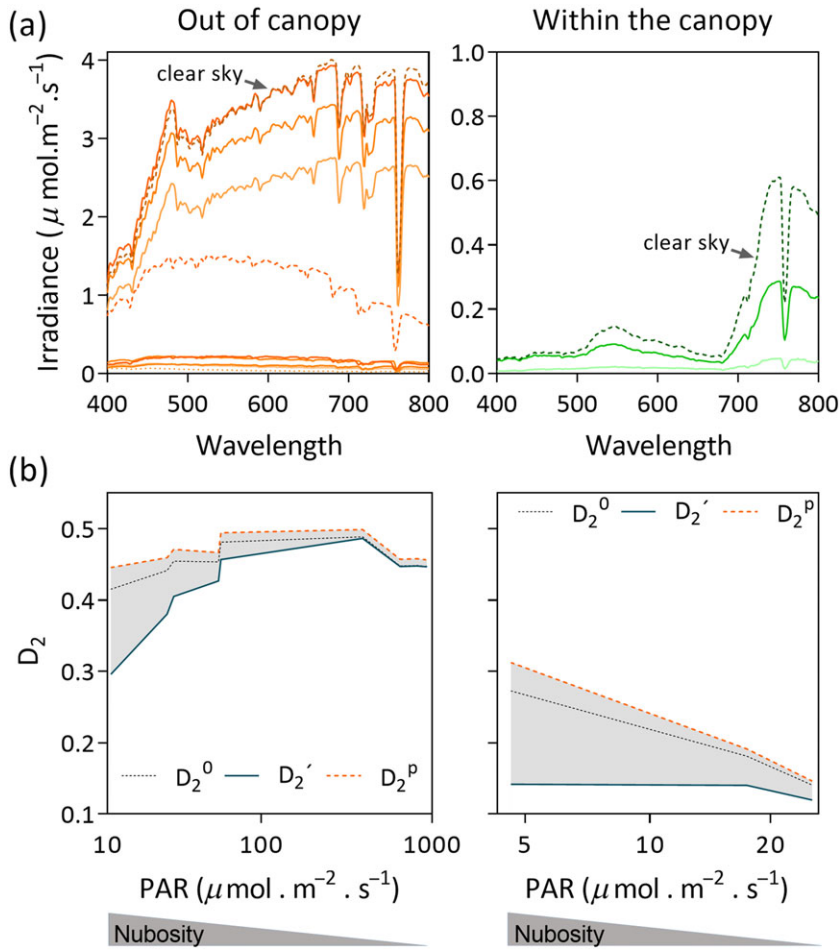


FIGURE 7 Nuclear D_2 out and within the canopy as affected by cloudiness. (a) Spectral photon distribution of the light out or within the canopy as affected by different degrees of nubosity. The curves that reach lower irradiances levels correspond to higher nubosity conditions. (b) Nuclear D_2 estimated by the original (D_2^0) or the perturbed model (D_2') compared with D_2 at photoequilibrium (D_2^P) for the conditions described in (a). The grey area shows the difference between D_2^P and D_2' [Colour figure can be viewed at wileyonlinelibrary.com]

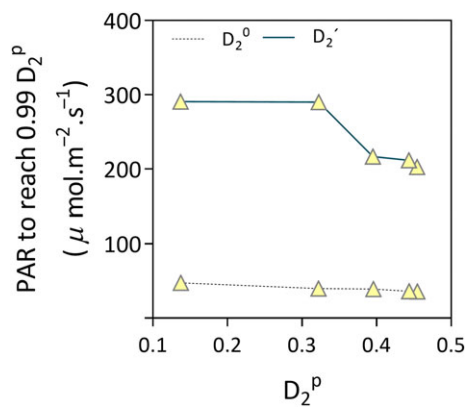


FIGURE 8 Irradiance required reaching 0.99 of D_2 at photoequilibrium for the spectral photon distribution recorded at different positions above or beneath the canopy. D_2 at photoequilibrium (D_2^P) was calculated for full sunlight and four heights beneath a wheat canopy and is plotted in abscissas (deeper shade is at the left and full sunlight at the right). Then irradiance was increased without changing the spectral composition to obtain either $D_2^0 = 0.99 D_2^P$ or $D_2' = 0.99 D_2^P$. The PAR values of the conditions that fulfil these equalities are indicated in ordinates for the calculations based on D_2^0 and on D_2' [Colour figure can be viewed at wileyonlinelibrary.com]

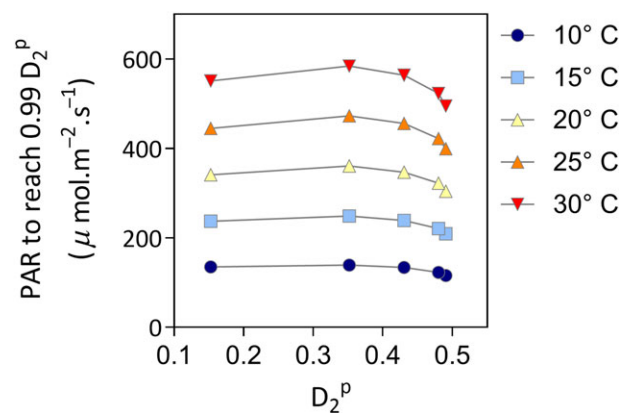


FIGURE 9 Higher irradiances are necessary to approach photoequilibrium under warmer temperatures. D_2 at photoequilibrium (D_2^P) was calculated for full sunlight and four heights beneath a wheat canopy and is plotted in abscissas (deeper shade is at the left and full sunlight at the right). Then irradiance was increased without changing the spectral composition to obtain $D_2 = 0.99 D_2^P$, where was estimated with the three-state model in combination with k_{r1} and k_{r2} values corresponding to the indicated temperatures (Jung et al., 2016; Legris et al., 2016). The PAR values of the conditions that fulfil these equalities are indicated in ordinates [Colour figure can be viewed at wileyonlinelibrary.com]

The cellular model of phyB was originally developed for etiolated seedlings exposed to continuous light within the red and far-red wavebands (Klose et al., 2015). The model was successful to account

for physiological responses during de-etiolation. However, the aim of the current work is to analyse phyB dynamics in de-etiolated seedlings that adjust their body architecture to the presence of neighbours. This

implies a number of differences, including the exposure of the seedlings to white light, which activates the blue-light sensory receptors cryptochromes, in addition to phytochromes. Furthermore, the daily cycles involve periods of light (photoperiod, day) and darkness (night), which provides a cue to synchronize circadian rhythms. There is no evidence in the literature to suspect that these differences might affect the photochemical reactions. However, there is evidence that circadian rhythms affect phyB dynamics (Bognár et al., 1999; Kircher et al., 2002). Furthermore, the cellular context can affect P_{fr} to P_r thermal reversion. This could occur via changes in the phosphorylation status of the phyB molecule (Medzihradzky et al., 2013) and changes in the status of phyB interacting partners such as the transcriptional regulators called phytochrome interacting factors (Smith et al., 2017) or the photoperiodic control of hypocotyl 1 protein (Enderle et al., 2017), all of which reduce the rate of thermal reversion. Actually, phyB synthesized in vitro is much less stable than phyB in vivo (Legris et al., 2016), and it has been proposed that phyB is protected from thermal reversion within NBs (Klose et al., 2015; Rausenberger et al., 2010; Van Buskirk et al., 2014). A complete reparameterization of the cellular model to accurately capture phyB dynamics in de-etiolated seedlings would require detailed information to calculate all the rates, which is beyond the scope of this work. Therefore, we evaluated the model parameters that would be most influential on the estimation of D_2 and observed that these are actually the rate of D_1 to D_0 dark reversion (k_{r1}), the rate of D_1 NB association (k_{31}), and the rate of D_1 NB dissociation (k_{41} ; Figure 1). Then we evaluated how the variations in these three parameters affected the estimation of hypocotyl growth rate in de-etiolated seedlings by using a growth model that incorporates D_2 values. The optimized values of k_{r1} and k_{41} were higher and those for k_{31} were lower than those used in the model optimized for etiolated seedlings (Figure 2). Because these values were adjusted individually, the correction factors are larger than if we considered the combined effects. Both a larger k_{41} and a lower k_{31} would reduce the proportion of phyB in NBs, and we actually observed a smaller proportion that predicted by the original model (Figure 3). Because phyB in NBs is protected from thermal reversion, the three modifications would go in the direction of increased apparent thermal reversion in our system. Therefore, the reduced stability of D_1 would actually be the result of the combined effects of approximately four-fold lower levels of phyB protected in NBs (from Figure 3a) and an approximately two-fold higher k_{r1} .

The observed phyB dynamics under field conditions has implications for phyB function. At first glance, the exquisite sensitivity of phyB-mediated perception of subtle light signals of nonshading neighbouring vegetation and the ability of phyB to act as a temperature sensor do not appear easy to reconcile. Here, we show that these two aspects of phyB activity occur in different scenarios. By definition, the detection of nonshading neighbours occurs in plants fully exposed to sunlight and actually ignores the light fluctuations at the extremes of the photoperiod (Casal, 2013). Under these conditions of high irradiance, phyB activity would be close to photoequilibrium and therefore affected mainly by the red/far-red ratio. Conversely, temperature sensing by phyB would occur in plants that are already shaded or transiently exposed to cloudy weather and therefore receive permissive irradiances.

ACKNOWLEDGEMENTS

This work was supported by the University of Buenos Aires (Grant 20020100100437 to J. J. C.), the Agencia Nacional de Promoción Científica y Tecnológica (Grant PICT-2015-1796 to J. J. C.), HFSP (Grant RGP0025/2013 to C. F.), FP7 Marie Curie Initial Training Network (Grant 316723 to R. W. S.), and Horizon 2020 (Grant 634942 to R. W. S.).

AUTHOR CONTRIBUTION

Sellaro R. planned and conducted field light and growth measurements; Smith R. W. planned and conducted light data analysis and phyB model variants; Legris M. conducted confocal experiments and designed the and applied a script for their analysis; Fleck C. and Casal J. J. proposed the original idea, designed, and supervised the research; and Casal J. J. wrote the manuscript with input from other authors.

ORCID

Romina Sellaro  <http://orcid.org/0000-0002-4412-1352>

Jorge J. Casal  <http://orcid.org/0000-0001-6525-8414>

REFERENCES

- Ballaré, C. L., & Pierik, R. (2017). The shade-avoidance syndrome: Multiple signals and ecological consequences. *Plant, Cell & Environment*, 11, 2530–2543.
- Ballaré, C. L., Sánchez, R. A. A., Scopel, A. L., Casal, J. J., & Ghera, C. M. (1987). Early detection of neighbour plants by phytochrome perception of spectral changes in reflected sunlight. *Plant, Cell and Environment*, 10, 551–557.
- Ballaré, C. L., Scopel, A. L., & Sánchez, R. A. (1990). Far-red radiation reflected from adjacent leaves: An early signal of competition in plant canopies. *Science*, 247, 329–332.
- Bauer, D., Viczián, A., Kircher, S., Nobis, T., Nitschke, R., Kunkel, T., & Nagy, F. (2004). Constitutive photomorphogenesis 1 and multiple photoreceptors control degradation of phytochrome interacting factor 3, a transcription factor required for light signaling in Arabidopsis. *Plant Cell*, 16, 1433–1445.
- Bognár, L. K., Hall, A., Adám, E., Thain, S. C., Nagy, F., & Millar, A. J. (1999). The circadian clock controls the expression pattern of the circadian input photoreceptor, phytochrome B. *Proceedings of the National Academy of Sciences of the United States of America*, 96, 14652–14657.
- Burgie, E. S., & Vierstra, R. D. (2014). Phytochromes: An atomic perspective on photoactivation and signaling. *The Plant Cell*, 26, 4568–4583.
- Casal, J. J. (2013). Photoreceptor signaling networks in plant responses to shade. *Annual Review of Plant Biology*, 64, 403–427.
- Casal, J. J., Sanchez, R. A., & Deregibus, V. A. (1986). The effect of plant density on tillering: The involvement of R/FR ratio and the proportion of radiation intercepted per plant. *Environmental and Experimental Botany*, 26, 365–371.
- Crepy, M. A., & Casal, J. J. (2015). Photoreceptor-mediated kin recognition in plants. *New Phytologist*, 205, 329–338.
- Deregibus, V. A., Sanchez, R. A., Casal, J. J., & Trlica, M. J. (1985). Tillering responses to enrichment of red light beneath the canopy in a humid natural grassland. *Journal of Applied Ecology*, 22, 199–206.
- Enderle, B., Sheerin, D. J., Paik, I., Kathare, P. K., Schwenk, P., Klose, C., & Hiltbrunner, A. (2017). PCH1 and PCHL promote photomorphogenesis in plants by controlling phytochrome B dark reversion. *Nature Communications*, 8, 2221.
- Franklin, K. A. (2008). Shade avoidance. *The New Phytologist*, 179, 930–944.

- Galvão, V. C., & Fankhauser, C. (2015). Sensing the light environment in plants: Photoreceptors and early signaling steps. *Current Opinion in Neurobiology*, 34, 46–53.
- Holmes, M. G., & Smith, H. (1977). The function of phytochrome in the natural environment—III. Measurement and calculation of phytochrome photoequilibria. *Photochemistry and Photobiology*, 25, 547–550.
- Jung, J. H., Domijan, M., Klose, C., Biswas, S., Ezer, D., Gao, M., ... Wigge, P. A. (2016). Phytochromes function as thermosensors in Arabidopsis. *Science*, 354, 886–889.
- Kaiser, E., Morales, A., & Harbinson, J. (2017). Fluctuating light takes crop photosynthesis on a rollercoaster ride. *Plant Physiology*, 176, pp.01250.2017
- Kelly, J. M., & Lagarias, J. C. (1985). Photochemistry of the 14-kilodalton Avena phytochrome under constant illumination in vitro. *Biochemistry*, 24, 6003–6010.
- Kim, J. I., Shen, Y., Han, Y. J., Park, J. E., Kirchenbauer, D., Soh, M.-S., ... Song, P. S. (2004). Phytochrome phosphorylation modulates light signaling by influencing the protein–protein interaction. *Plant Cell*, 16, 2629–2640.
- Kircher, S., Gil, P., Kozma-Bognar, L., Fejes, E., Speth, V., Husselstein-Muller, T., ... Nagy, F. (2002). Nucleocytoplasmic partitioning of the plant photoreceptors phytochrome A, B, C, D, and E is regulated differentially by light and exhibits a diurnal rhythm. *The Plant Cell*, 14, 1541–1555.
- Klose, C., Venezia, F., Hussong, A., Kircher, S., Schäfer, E., & Fleck, C. (2015). Systematic analysis of how phytochrome B dimerization determines its specificity. *Nature Plants*, 1, 15090.
- Koornneef, M., Rolf, E., & Spruit, C. J. P. (1980). Genetic control of light-inhibited hypocotyl elongation in *Arabidopsis thaliana* (L.) Heynh. *Z. Pflanzenphysiologie*, 100, 147–160.
- Legris, M., Klose, C., Burgie, E., Costigliolo, R. C., Neme, M., Hiltbrunner, A., ... Casal, J. J. (2016). Phytochrome B integrates light and temperature signals in Arabidopsis. *Science*, 354, 897–900.
- Legris, M., Nieto, C., Sellaro, R., Prat, S., & Casal, J. J. (2017). Perception and signalling of light and temperature cues in plants. *The Plant Journal*, 90, 683–697.
- López, P. M., Sadras, V. O., Batista, W., Casal, J. J., & Hall, A. J. (2017). Light-mediated self-organization of sunflower stands increases oil yield in the field. *Proceedings of the National Academy of Sciences of the United States of America*, 114, 7975–7980.
- Maddonni, G. A., Otegui, M. E., Andrieu, B., Chelle, M., & Casal, J. J. (2002). Maize leaves turn away from neighbors. *Plant Physiology*, 130, 1181–1189.
- Mancinelli, A. L. (1988). Some thought about the use of predicted values of the state of phytochrome in plant photomorphogenesis research. *Plant, Cell & Environment*, 11, 429–439.
- Mancinelli, A. L. (1994). The physiology of phytochrome action. In R. E. Kendrick, & G. H. M. Kronenberg (Eds.), *Photomorphogenesis in plants* (2nd ed.) (pp. 211–269). Dordrecht, The Netherlands: Kluwer Academic Publishers.
- Martínez-García, J. F. J., Galstyan, A., Salla-Martret, M., Cifuentes-Esquivel, N., Gallemí, M., & Bou-Torrent, J. (2010). Regulatory components of shade avoidance syndrome. *Advances in Botanical Research*, 53, 65–116.
- Medzihradsky, M., Bindics, J., Ádám, É., Viczián, A., Klement, É., Lorrain, S., ... Nagy, F. (2013). Phosphorylation of phytochrome B inhibits light-induced signaling via accelerated dark reversion in Arabidopsis. *Plant Cell*, 25, 535–544.
- Michaud, O., Fiorucci, A., Xenarios, I., & Fankhauser, C. (2017). Local auxin production underlies a spatially restricted neighbor-detection response in Arabidopsis. *Proceedings of the National Academy of Science*, 114, 7444–7449.
- Moriconi, V., Binkert, M., Costigliolo, C., Sellaro, R., Ulm, R., & Casal, J. J. (2018). Perception of sunflecks by the UV-B photoreceptor UV RESISTANCE LOCUS8. *Plant Physiology*, 177, 75–81.
- Pantazopoulou, C. K., Bongers, F. J., Kupers, J. J., Reinen, E., Das, D., Evers, J. B., ... Pierik, R. (2017). Neighbor detection at the leaf tip adaptively regulates upward leaf movement through spatial auxin dynamics. *Proceedings of the National Academy of Sciences*, 114, 7450–7455.
- Rausenberger, J., Hussong, A., Kircher, S., Kirchenbauer, D., Timmer, J., Nagy, F., ... Fleck, C. (2010). An integrative model for phytochrome B mediated photomorphogenesis: From protein dynamics to physiology. *PLoS One*, 5, e10721.
- Sellaro, R., Yanovsky, M. J., & Casal, J. J. (2011). Repression of shade-avoidance reactions by sunfleck induction of HY5 expression in Arabidopsis. *Plant Journal*, 68, 919–928.
- Smith, H. (2000). Phytochromes and light signal perception by plants—An emerging synthesis. *Nature*, 407, 585–590.
- Smith, H., Casal, J. J., & Jackson, G. M. (1990). Reflection signals and the perception by phytochrome of the proximity of neighbouring vegetation. *Plant, Cell and Environment*, 13, 73–78.
- Smith, H., & Holmes, M. G. (1977). The function of phytochrome in the natural environment III Measurement and calculation of phytochrome photoequilibrium. *Photochemistry and Photobiology*, 225, 547–550.
- Smith, H., & Whitelam, G. C. (1990). Phytochrome, a family of photoreceptors with multiple physiological roles. *Plant, Cell and Environment*, 13, 695–707.
- Smith, R. W., Helwig, B., Westphal, A. H., Pel, E., Borst, J. W., & Fleck, C. (2017). Interactions between phyB and PIF proteins alter thermal reversion reactions in vitro. *Photochemistry and Photobiology*, 93, 1525–1531.
- Trupkin, S. A., Legris, M., Buchovsky, A. S., Rivero, M. B. T., & Casal, J. J. (2014). Phytochrome B nuclear bodies respond to the low red to far-red ratio and to the reduced irradiance of canopy shade in Arabidopsis. *Plant Physiology*, 165, 1698–1708.
- Van Buskirk, E. K., Reddy, A. K., Nagatani, A., & Chen, M. (2014). Photobody localization of phytochrome B is tightly correlated with prolonged and light-dependent inhibition of hypocotyl elongation in the dark. *Plant Physiology*, 165, 595–607.
- Yanovsky, M. J., Casal, J. J., & Whitelam, G. C. (1995). Phytochrome A, phytochrome B and HY4 are involved in hypocotyl growth responses to natural radiation in Arabidopsis: Weak de-etiolation of the phyA mutant under dense canopies. *Plant, Cell and Environment*, 18, 788–794.
- Zhang, J., Stankey, R. J., & Vierstra, R. D. (2013). Structure-guided engineering of plant phytochrome B with altered photochemistry and light signaling. *Plant Physiology*, 161, 1445–1457.

SUPPORTING INFORMATION

Additional supporting information may be found online in the Supporting Information section at the end of the article.

How to cite this article: Sellaro R, Smith RW, Legris M, Fleck C, Casal JJ. Phytochrome B dynamics departs from photoequilibrium in the field. *Plant Cell Environ*. 2018;1–12. <https://doi.org/10.1111/pce.13445>